# CHAPTER 4

# RESULTS AND DISCUSSION

## 4.1 Characteristic of hydroxyapatite powders.

### 4.1.1 Ca/P ratios and impurities in starting materials

Amount of Ca, P. and other impurities were characterized and reported in Table 4.1

**Table 4.1** Chemical compositions and impurities of MP, TP and CHA powders

| Composition | Starting materials | | |
|---|---|---|---|
| | MP | TP | CHA |
| % Ca | 38.91 | 38.15 | 39.16 |
| % P | 18.20 | 17.57 | 18.15 |
| Ca : P mole ratio | 1.64 | 1.67 | 1.66 |
| Impurities, | | | |
| % Mg | 0.83 | 0.64 | 0.01 |
| % Fe | 0.04 | 0.07 | 0.06 |
| Zn | 120 | <50 | <50 |
| Cu | 13 | 6 | 4 |
| Mn | 5 | 5 | 5 |
| Heavy metals, ppm | | | |
| Cd | <0.5 | <0.5 | <0.5 |
| Pb | <5 | <5 | <5 |
| Hg | <1 | <1 | <1 |
| As | <0.5 | <0.5 | <0.5 |

Data from : Department of Science and Services

Mineral Assay and Services

Table 4.1. shows chemical composition and amount of impurities. Ca:P ratio of MP was 1.64 and CHA was 1.66, respectively. It was indicated that MP and CHA were calcium deficient hydroxyapatite. But in TP ,Ca:P ratio was 1.67 be stoichiometric value. Amount of impurities in TP and CHA were less than MP. These might result from impuities be controlled during the chemical process. Heavy metal in MP,TP and CHA were very low and lower than the maximum limit in ASTM 1185-88 in Appendix G.

### 4.1.2 Phase present of Starting powders

XRD pattern of MP, TP, CHA powder showed in Fig. 4.1. It was found that the phase of all powders be hydroxyapatite, no second phase presented the sharp peak of TP and CHA came from crystallinity after sintering at high temperature that make it easily to indentifying.

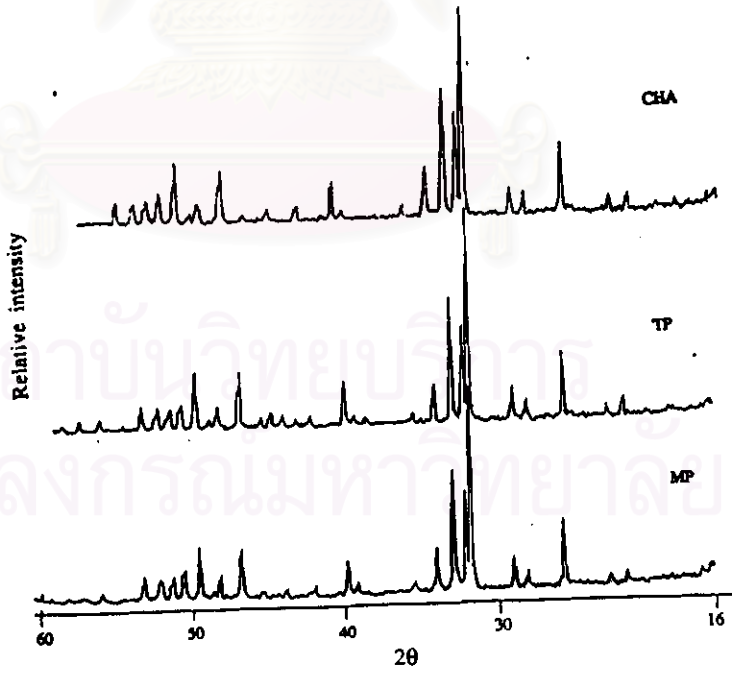


**Fig.4.1.** XRD patterns of MP, TP and CHA powder

### 4.1.3 Functional groups

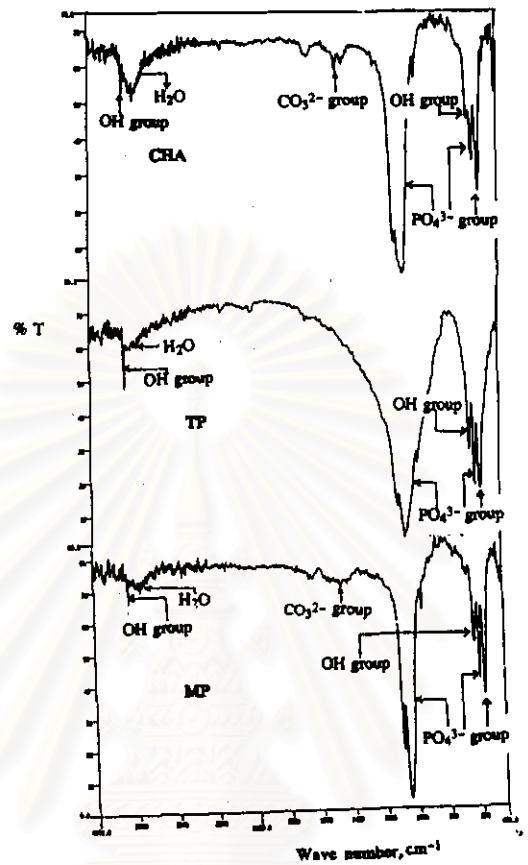


**Fig. 4.2** Infrared absorption spectra of MP, TP and CHA powder

From infrared absorption spectra shown the $PO_4^{3-}$ vibration and OH stretching and vibration which can be interpreted as the sharp peak at 3600 and 630 $cm^{-3}$ were assign to OH streching. Peak at 600,1080 and 1100 were assign to $PO_3^{2-}$. Small peak at 1480 and 1510 were relevant to $CO_3^{2-}$ group.

### 4.1.4 Surface area and pore volume

Specific surface area and pore volume of MP, TP and CHA were shown in Table 4.2

**Table 4.2** Pore volume and specific surface area of MP, TP and CHA powder

| Materials | Pore volume ($cm^3/g$) $10^{-2}$ | Surface area ($m^2/g$) |
|---|---|---|
| MP | 0.16 | 2.66 |
| TP | 9.30 | 73.62 |
| CHA | 6.04 | 47.42 |

The results from Table 4.2 indicated that MP had low specific surface area than TP and CHA as well as pore volume because TP and CHA had the smaller particle sizes than MP.

### 4.1.5 Density

The density of MP, TP and CHA powder were shown in Table 4.3

**Table 4.3** Density of MP, TP and CHA powder

| Materials | Density (g/cm3) |
|---|---|
| MP | 3.1719 |
| TP | 2.9953 |
| CHA | 3.0186 |

Density of MP was more than TP and CHA because of impurities embeded in powder. For TP may also contain blind pores which are totally encapsulated by the particle and will effectively reduce the particle's density.

### 4.1.6 Particle size distribution

Particle size of MP, TP and CHA reported from particle size analyzer was shown in Fig. 4.3-4.5

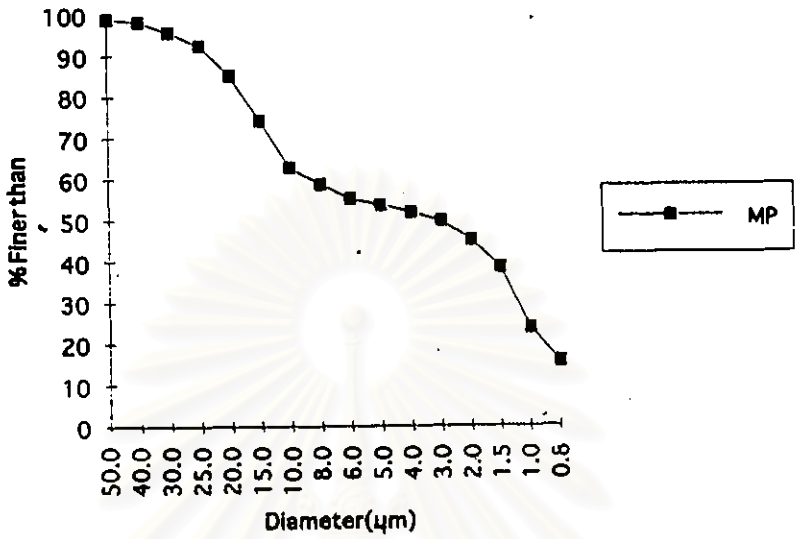


**Fig. 4.3** Particle size distribution of MP

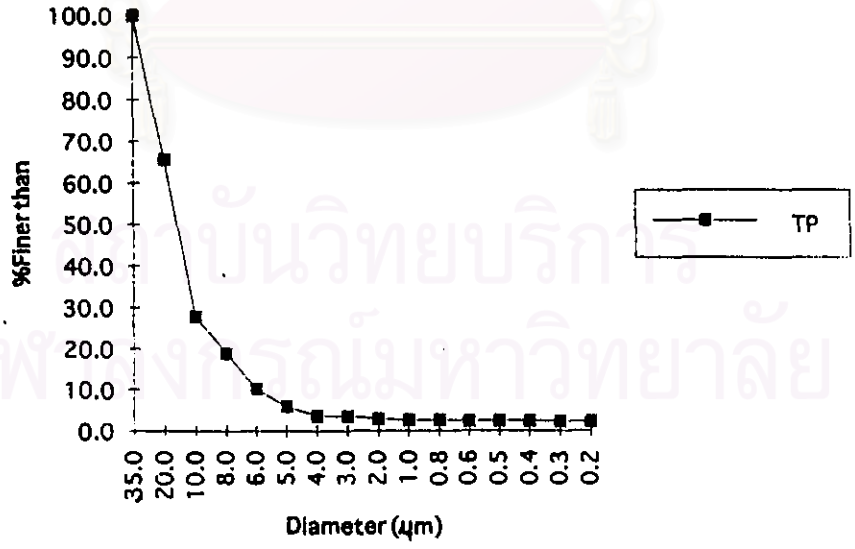


**Fig. 4.4** Particle size distribution of TP

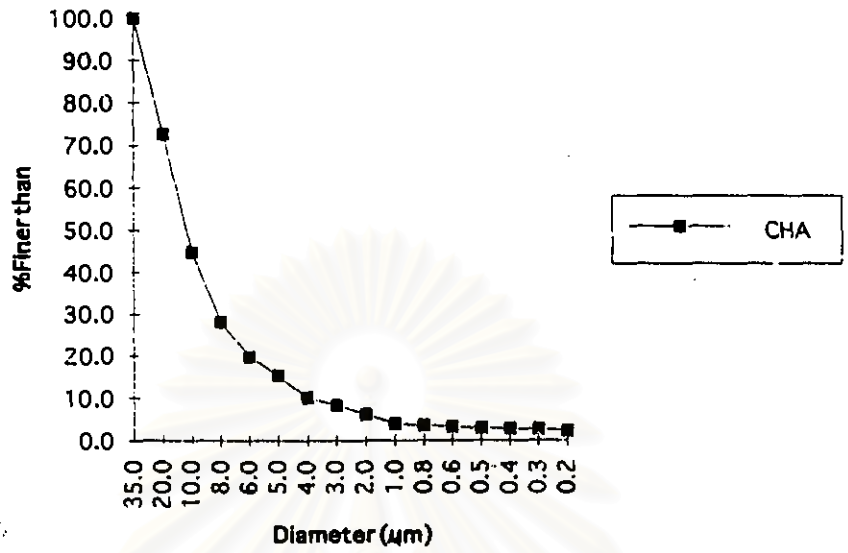


**Fig. 4.5** Particle size distribution of CHA.

From particle size distribution curves could be interpreted that

MP at $P_{50}$ finer than 3 μm.

TP at $P_{50}$ finer than 15 μm.

CHA at $P_{50}$ finer than 12 μm.

The result showed that MP particle finer than TP and CHA. But from surface area of MP, TP and CHA powder. TP and CHA had more surface area than MP that was indicated TP and CHA finer than MP. More surface area made surface active in particles and caused agglomerates between the particles. So, the results of particle size distribution may come from agglomerate of TP / CHA particles. To prove this effect, particle morphology of MP, TP and CHA powders should be detected.

### 4.1.7 Particle morphology

Transmission electron microscope of MP, TP and CHA powders were shown in Fig. 4.6–4.8. MP particles were irregular shape and relative large size. TP and CHA particles were ellipsoidal shape and particle size were very small. TP shown agglomerates of particle more than CHA.

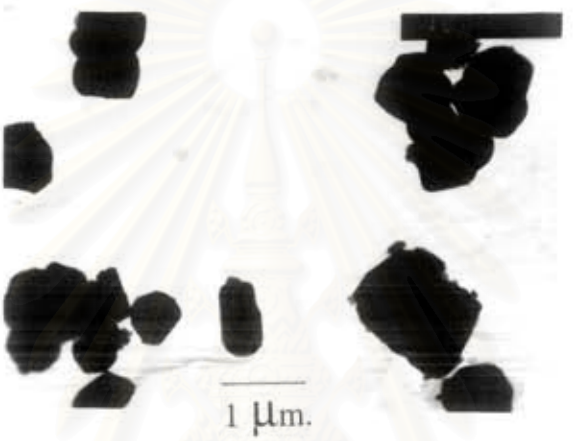


**Fig. 4.6** TEM photomicrograph of MP (x 10,000)

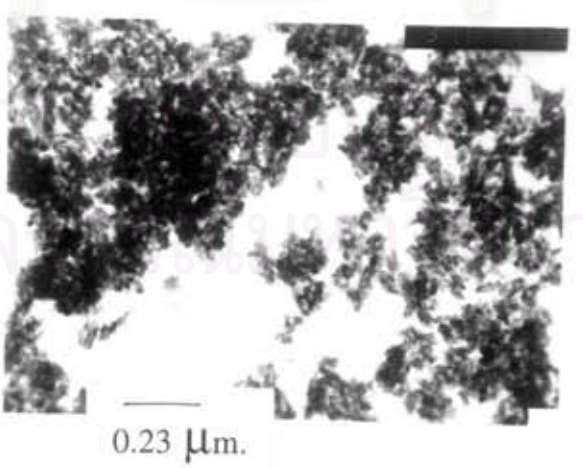


**Fig. 4.7** TEM photomicrograph of TP (x 37,000)

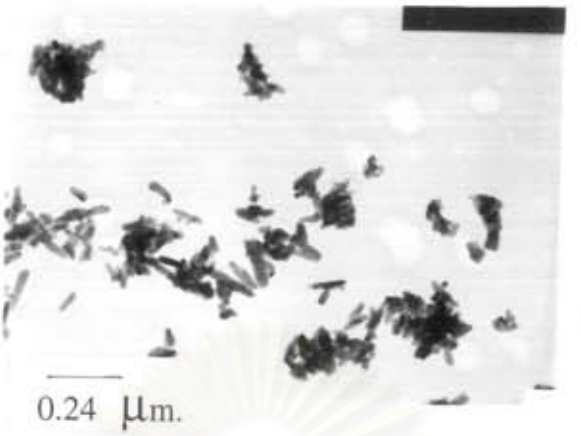


**Fig. 4.8** TEM photomicrograph of CHA (x 37,000)

## 4.2 Characterization of cellulose sponge and polyurethane foam

### 4.2.1 Inner structure

From optical microscope, inner structure of sponges and foams were shown in Fig. 4.9 and 4.10. Pores within sponges / foams were interconnecting pores.

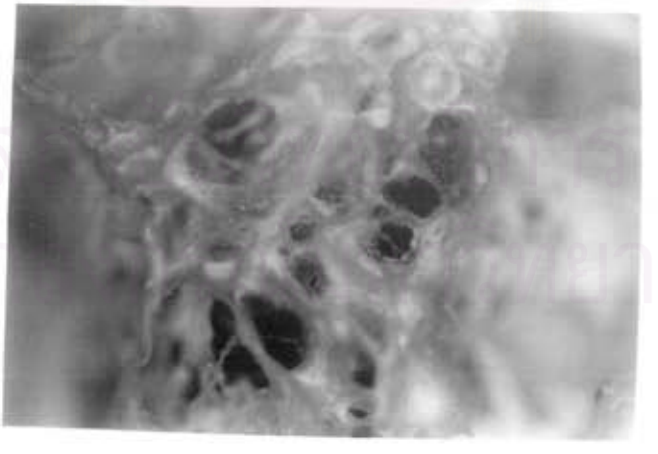

**Fig. 4.9** Inner struture of cellulose sponge (x 16)

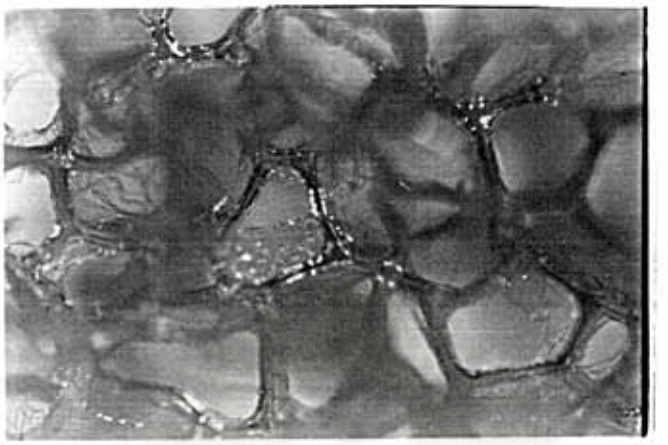

**Fig. 4.10** Inner structure of polyurethane foam (x 16)

From SEM, structure of cellulose sponge and foam were shown in Fig. 4.11-4.12 and displayed interconnecting pore as well as results from optical microscope.

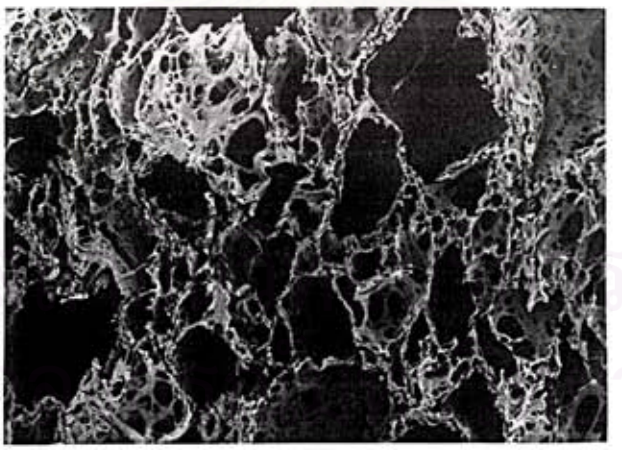

**Fig. 4.11.** SEM micrograph of cellulose sponge (x15)

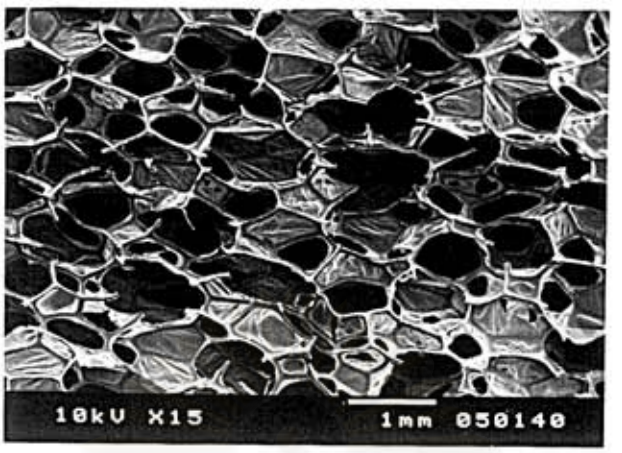


**FIg. 4.12.** SEM micrograph of polyurethane foam. (x15)

### 4.2.2 Temperature for burn out organic matter in sponges/foams

4.2.2.1 Differential thermal analysis (DTA) and thermal gravimetric analysis (TGA)

DTA and TGA curves of cellulose sponge at heating rate 10°C /min. in air atmosphere and temperature 20-1500°C were shown in Fig. 4.11 But the experiment on polyurethane foams was skipped. Because these foams caused cyanide gas during oxidation process. Cyannide is dangerous for human.

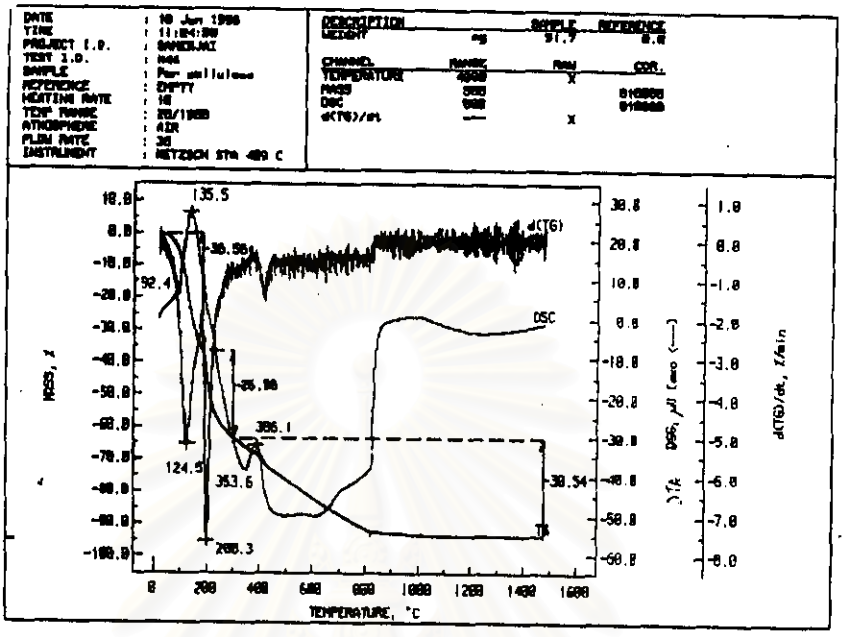


**Fig. 4.13.** DTA and TGA thermograms of cellulose sponges.

From DTA data, Cellulose showed a minor endothermic reaction just above 100°C, corresponding to the loss of adsorbed water, followed by a major endothermic-exothermic sequence just above 300°C. At these temperature range, TGA had the rapid weight loss occuring in concern with the large endothermic reaction. These data were interpreted as being indicative of a two step reaction with the change in the mechanism occuring at about the transition point (above 300°C), the predominate path way results in reduction in the degree of polymerization, the elimination of water, and the generation of carbonmonoxide, carbon dioxide, free radicals carbonyl, carboxyl, and hydroperoxide groups. The slower loss then occurs at 400°C to 820°C may be the dissociation of $Mg(OH)_2$ to MgO and $H_2O$

4.2.2.2 Differentials thermal analysis (DSC)

DSC for polyurethane is skipped due to its toxicity. However for polyurethane Ching and Surrel, 1993 reported that the burn out temperature was 400°C.

4.2.2.3 Phase analysis in cellulose sponge ash

% Ash of cellulose = 5.63

(Temperature 900°C / 1 h. in Pt crucible from starting cellulose sponge 2 g.)

% Residues of polyurethane foam = 0.27

(Temperature 400°C /1 h. in Pt crucible, from starting polyurethane foam 2 g.)

After firing, ash of celluloe was taken to perform X-ray diffraction to detect phase. The result was shown in Fig. 4.14

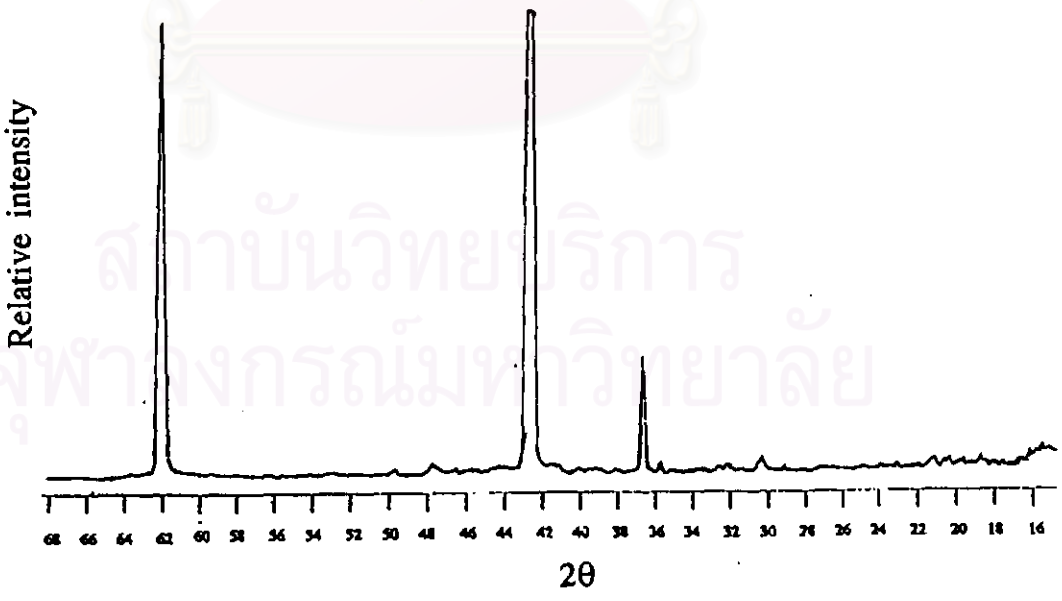


**Fig. 4.14** XRD pattern of cellulose sponge ash.

From XRD pattern of cellulose ash compared with X-ray diffraction card in Appendix C was indicated that the major composition was MgO with little impurity which can't interprete by XRD method because of the low intensity of peaks.

4.2.2.4 Impurities from sponges / foam

Scanning electron microscope (SEM-EDX) used to study impurities within cellulose sponges after firing at 900°C / 1 h. The results shown major phase be Mg with impurities such as Ca and Al.


**Fig. 4.15.** SEM-EDX of cellulose sponges ash.

Polyurethane foam melted and form glassy phase when firing at high temperature. So, the SEM-EDX of MP, TP and CHA slip compared with MP, TP and CHA sintered product were studied. The result were not differ in MP, TP, and CHA. Major elements in slips and product were Ca and P with impurities C and O. SEM-EDX of CHA 47.5% slip and sintered product were shown in Fig 4.16.

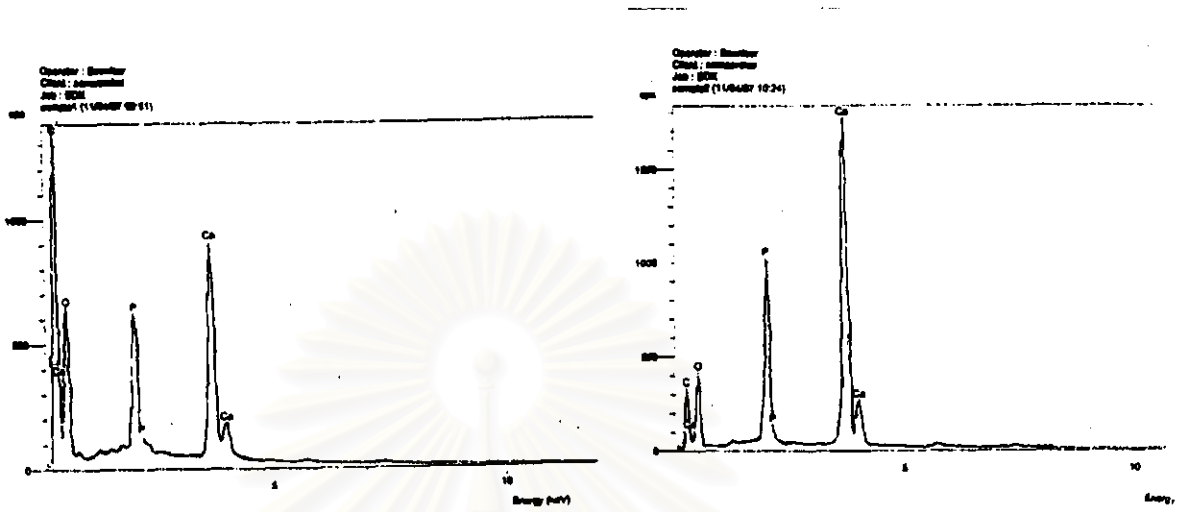

(A) (B)

**Fig. 4.16.** SEM-EDX of

**(A)** CHA slip **(B)** CHA sintered specimen

## 4.3. Rheological properties

Because of the more solid adding to the slip system, deflocculant must be added to the system to adjust suitable viscosity . So the relationship between amount of deflocculant (g.) and viscosity (poise) were plotted, these curves showed that slips were thixotropic (pseudoplastic).

### 4.3.1 MP Slip

MP 70 % solid with 15% w/v dispex A40 was prepared to slip. Dispex dosages were plotted against viscosity of system followed the standard ASTM D 2196-86 shown in Fig. 4.17

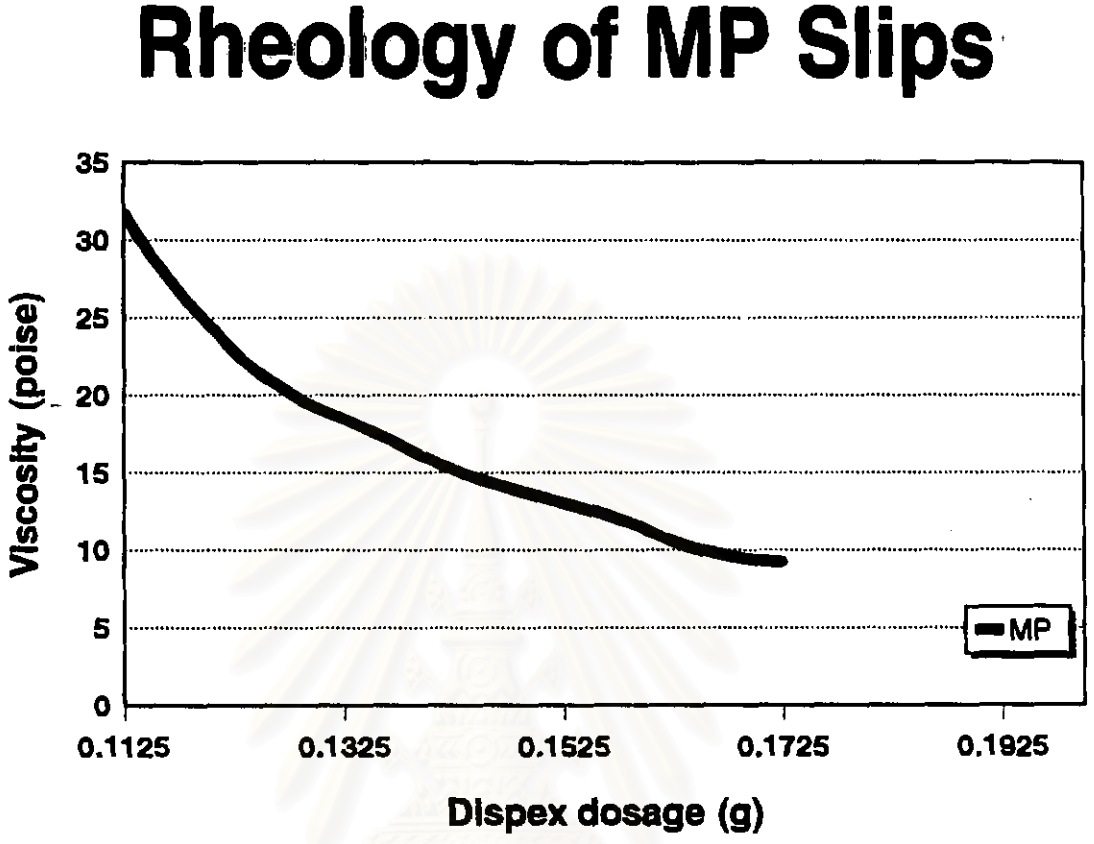


**Fig. 4.17.** Rheological curve of MP 70% solid-15%w/v dispex A 40 (Brookfield viscometer, spindle no. 3, 20 rpm.,temperature 31°C)

### 4.3.2 TP Slip

TP 47.5% with 27%w/v dispex were prepared to slips. Rheological curve followed the standard ASTM D 2196-86 was performed and the results were shown in Fig. 4.18

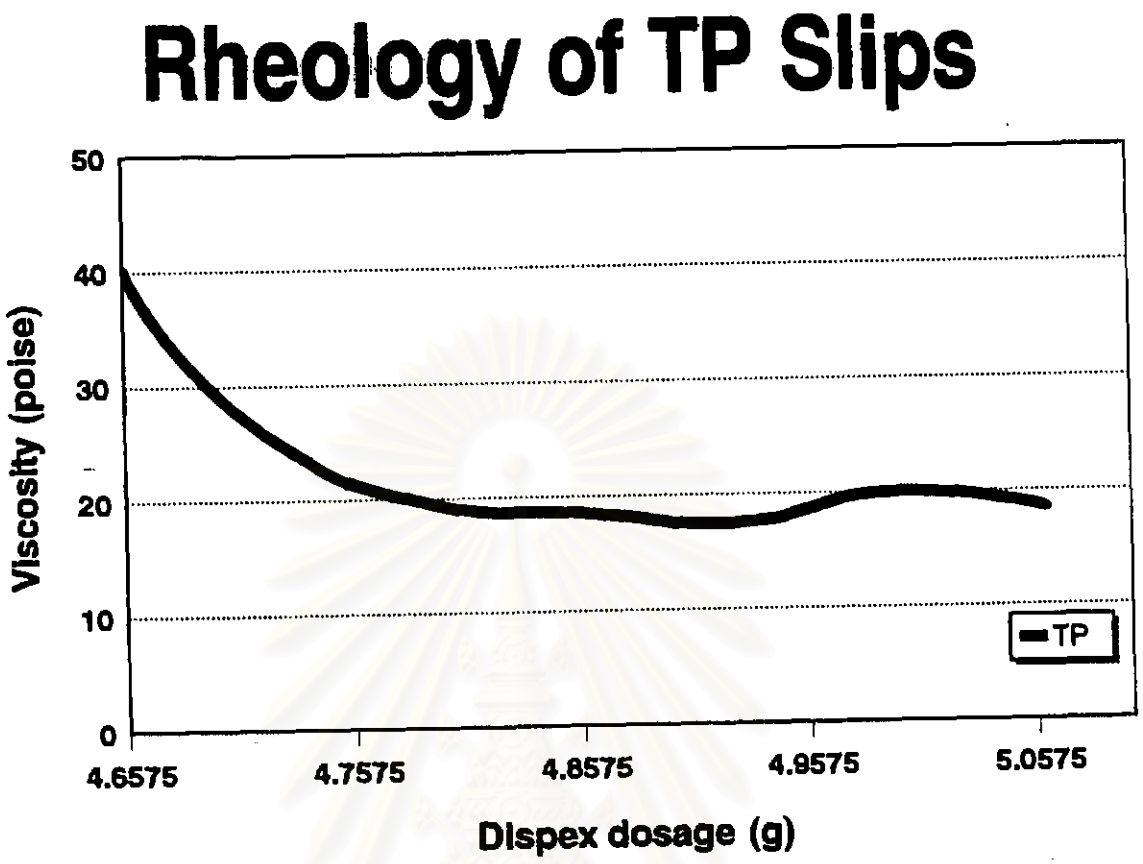


**Fig. 4.18.** Rheological curve of TP 47.5% - 27% w/v dispex A. 40 (Brookfield viscometer, spindle No. 3, 20 rpm, temperature 31°C)

### 4.3.3 CHA slip

CHA 47.5% solid with dispex A 40 concentration 25 %w/v was used as deflocculant. Rheological curve of CHA 47.5% followed ASTM D 2196-86 were ploted and shown in Fig. 4.19.

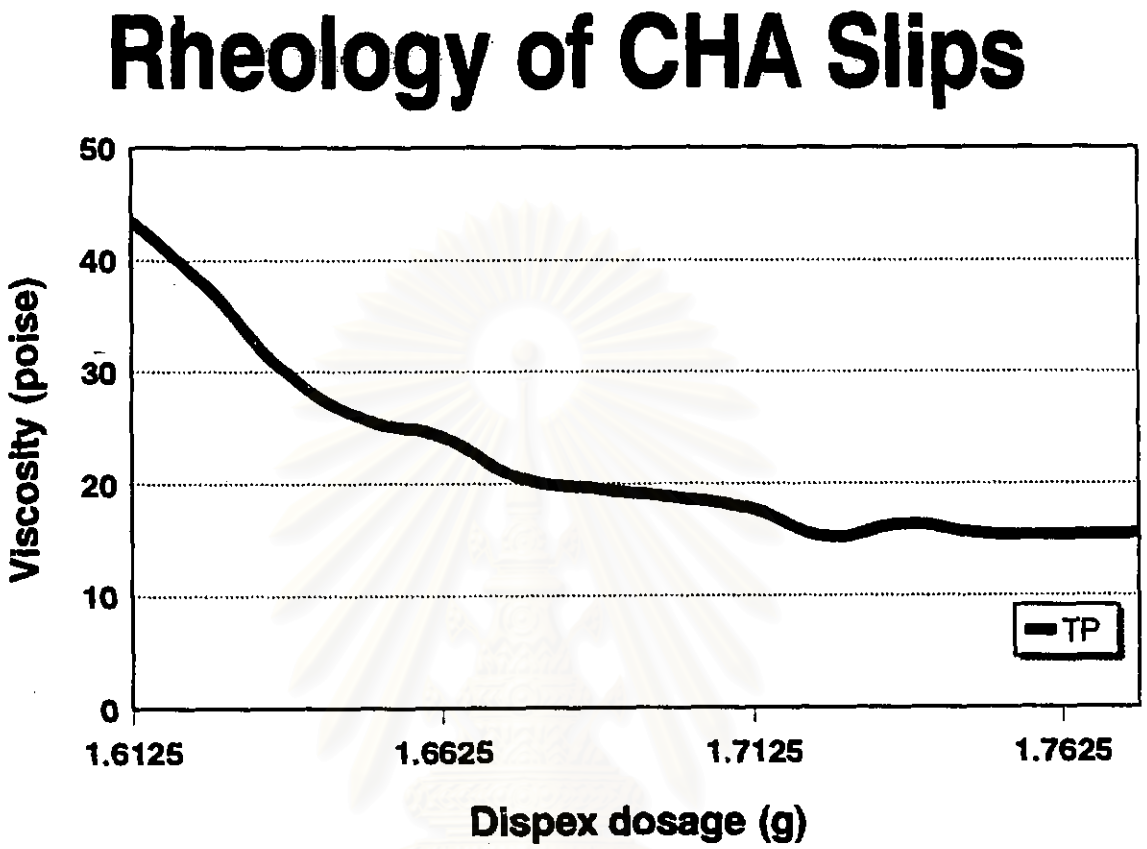


**Fig. 4.19.** Rheological curve of CHA 47.5%-25% w/v. dispex A 40 (Brookfield viscometer, spindle No. 3, rpm = 20 temperature 31°C)

For TP and CHA viscosity curve, TP used amount of dispex more than CHA. This may be the consistency in TP slip. Dispex dosage was minimum in MP slip. These results can be shown in Fig. 4.20. The effect of these behavior came from the small particle size which cause surface active in particle. Particle were formed agglomerate which must use more dispex dosages( MP < TP < CHA ) to solve this problem.

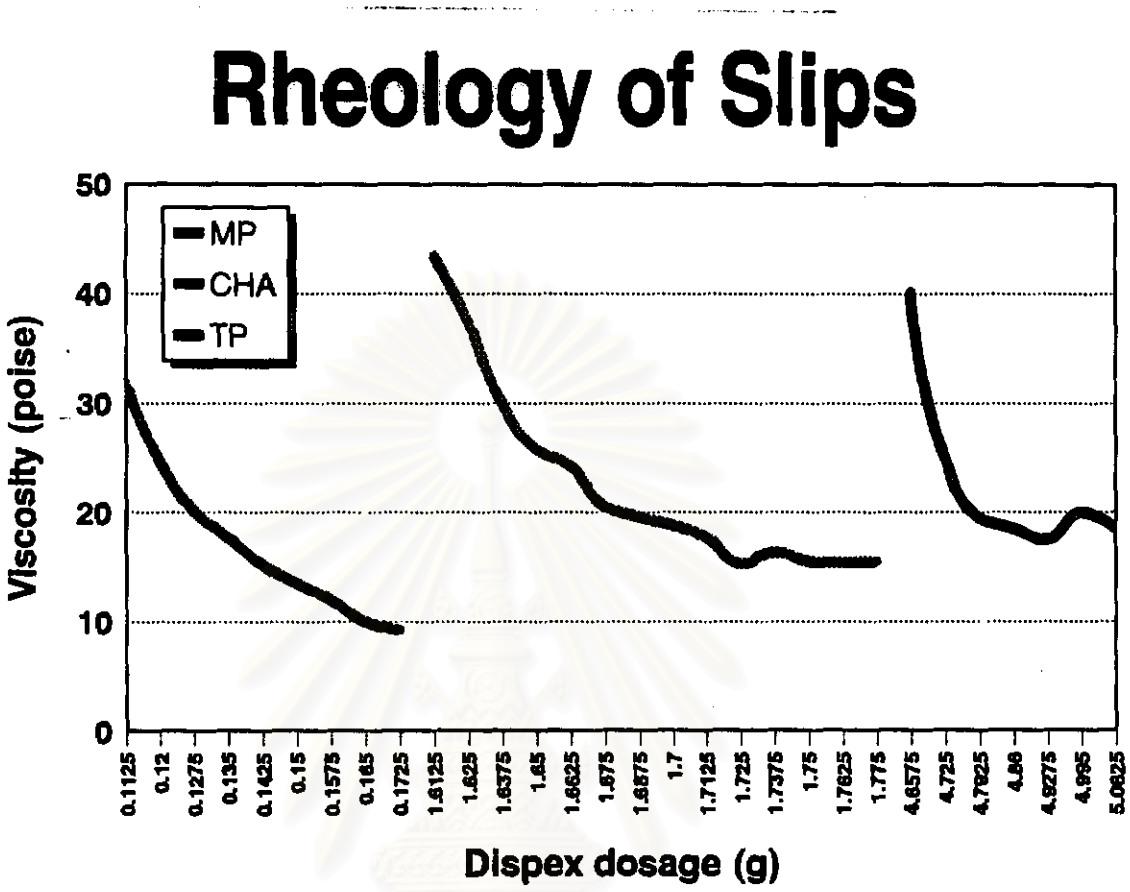


**Fig. 4.20.** Rheological curve of MP, TP and CHA with different dispex dosage (Brookfield viscometer, spindle No. 3 rpm = 20 temperature 31°C)

### 4.3.4 Slip properties

The properties of MP, TP and CHA slips were studied as shown in Table 4.4

**Table 4.4.** MP, TP and CHA slip properties

| Type of slip | Slip density ($g/cm^3$) | pH of slip | Viscosity (poise) after adding additives |
|---|---|---|---|
| MP 60% | 1.56 | 10.40 | 2.90 |
| MP 70% | 1.78 | 10.47 | 8.95 |
| TP 47.5% | 1.37 | 8.39 | 22.30 |
| CHA 47.5% | 1.42 | 8.21 | 28.55 |

The role of deflocculant (dispex A 40) in dispersing MP, TP and CHA particles occurred by the mechanism of withdrawing hydronium ions ($H^+$) from OH groups in hydroxyapatite particle. That induced the negative charge in the particles. Particle in water repelled each other made low viscosity in slip and kept the stable system. This effect can be indicated from pH of slips which had only starting materials, distilled water and deflocculant. The pH of such materials were between 8–10.

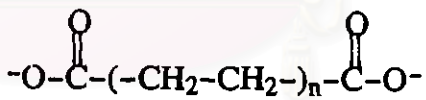

**Fig. 4.21.** Structure of dispex A. 40 (The ammonium salt of polycarboxylic acid)

Solid contents in slip were decreased because of water within additive mixture be added into slip system. So, real solid in slip system must be determined.

**Table 4.5.** Real solid content in slip system

| Materials | Real % solids | Remark |
|---|---|---|
| MP (60%) | 54.55 | Very low viscosity |
| MP (70%) | 59.41 | Flowable and more consistency than MP (60%) |
| TP (47.5%) | 41.61 | Flowable |
| CHA (47.5%) | 43.04 | Flowable |

## 4.4 Characterization of porous hydroxyapatite specimens

### 4.4.1 Specimens after sintering

Specimens of MP, TP and CHA from the origin replicated from cellulose sponge or polyurethane foam are shown in Fig. 4.22. Specimens were the same feature in cellulose sponge replicated and different from those of polyurethane replicated. MP, TP and CHA specimens were fabricated to porous specimens except those from MP 60% solid in cellulose sponge were broken during the sintering process.

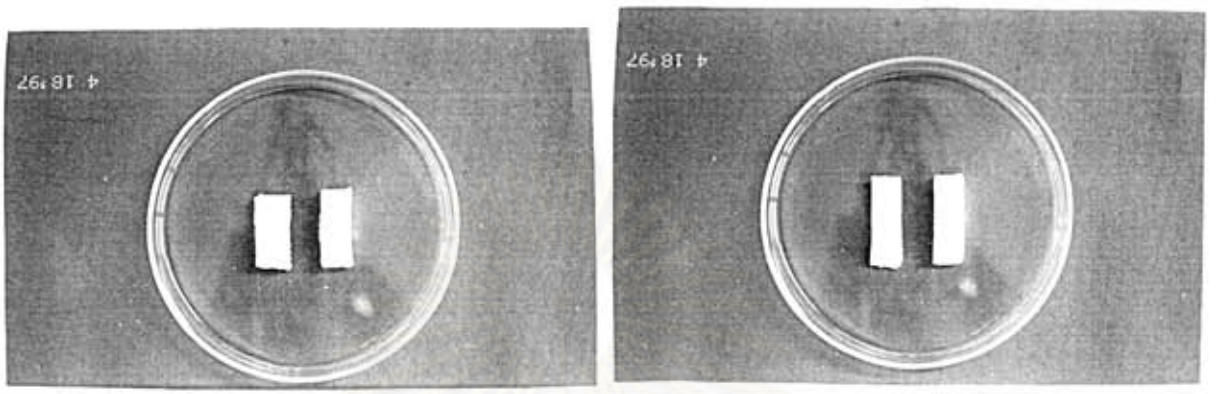

(A) (B)

**Fig. 4.22.** Porous specimens replicated from
**(A)** Cellulose sponge **(B)** Polyurethane foam

### 4.4.2 Sintered characterization

4.4.2.1 Phase identification

From XRD pattern from Fig. 4.23-4.26 showed XRD pattern of sintered specimens of MP (60%), MP (70%), TP (47.5%) and CHA (47.5%). The d spacing from these XRD pattern compared with X-ray diffraction card of hydroxyapatite in appendix A. was identified as hydroxyapatite and no second phase was found.

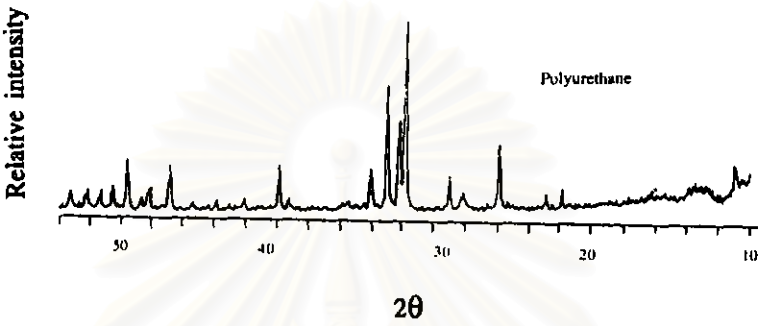


**Fig. 4.23.** XRD patterns of MP (60% solid) specimens

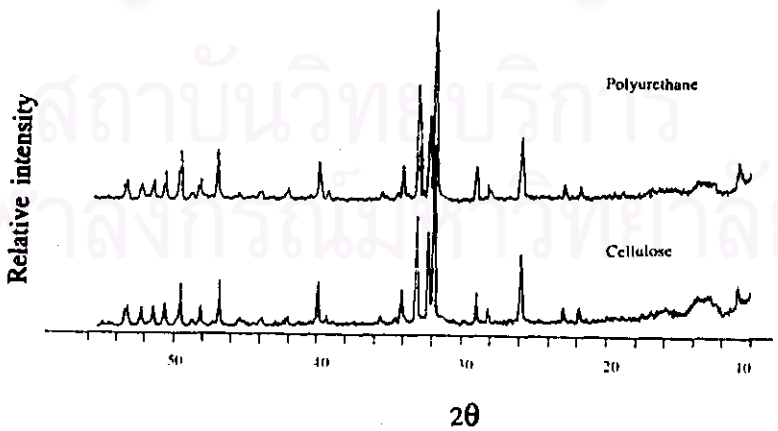


**Fig. 4.24.** XRD patterns of MP (70% solid) specimens

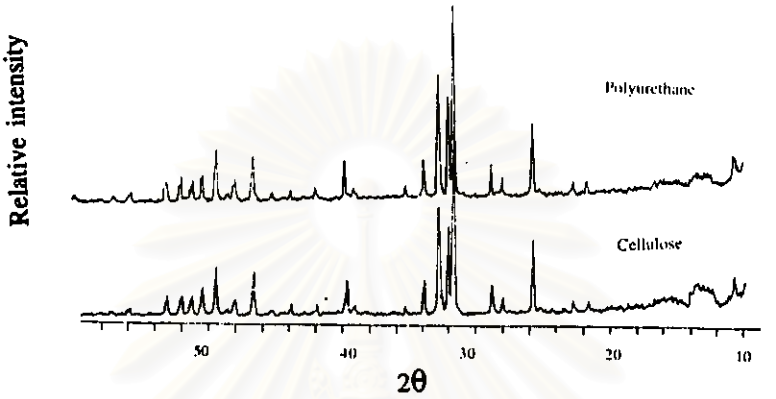


**Fig. 4.25.** XRD patterns of TP specimens

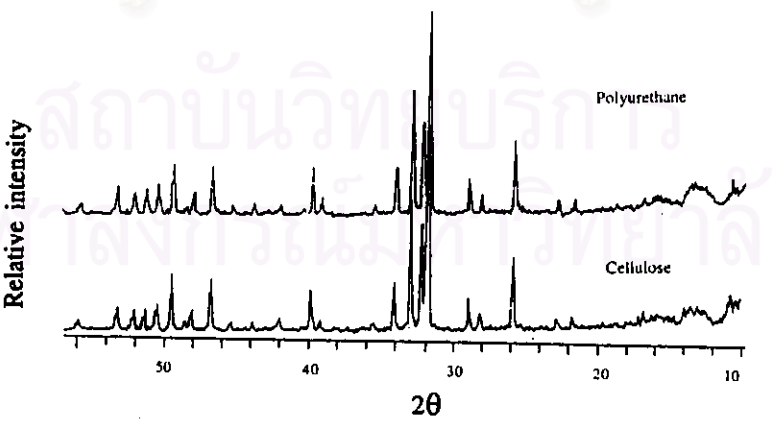


**Fig. 4.26.** XRD patterns of CHA specimens.

### 4.4.2 Functional groups

Functional group from FT-IR MP (60%), MP (70%), TP and CHA were shown in Fig. 4.27-4.30 indicating that OH groups existed in specimens after sintering. Functional groups of same materials but different sponge supporter shown the same IR pattern. $CO_3^{2-}$ group was disappeared and formed $CO_2$ during sintering at high temperature.

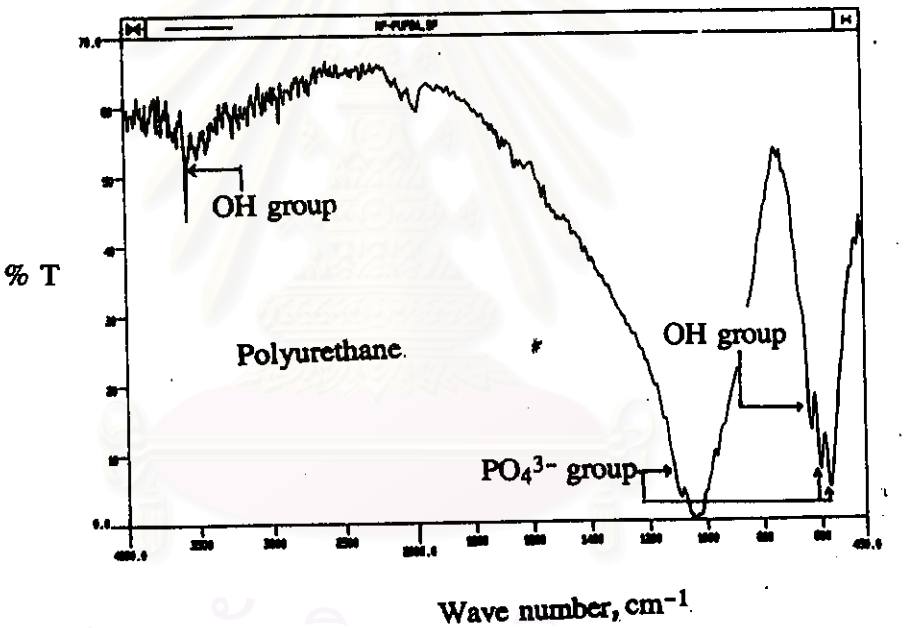


**Fig. 4.27.** Functional groups of MP (60% solid) specimens

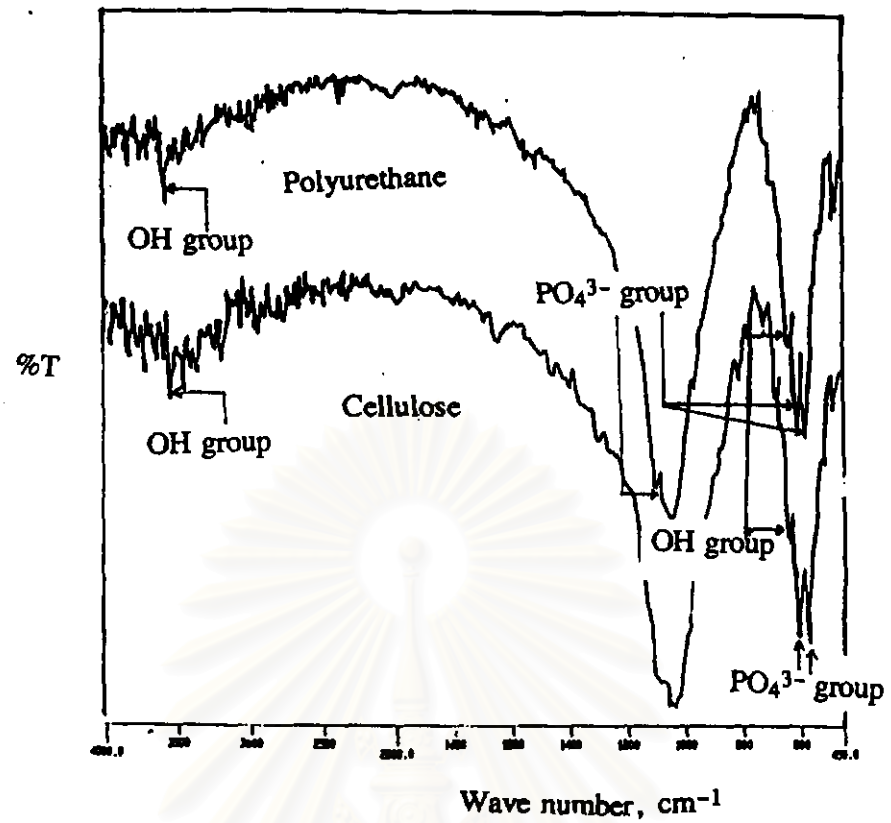


**Fig. 4.28.** Functional groups of MP (70% solid) specimens on different supporter.

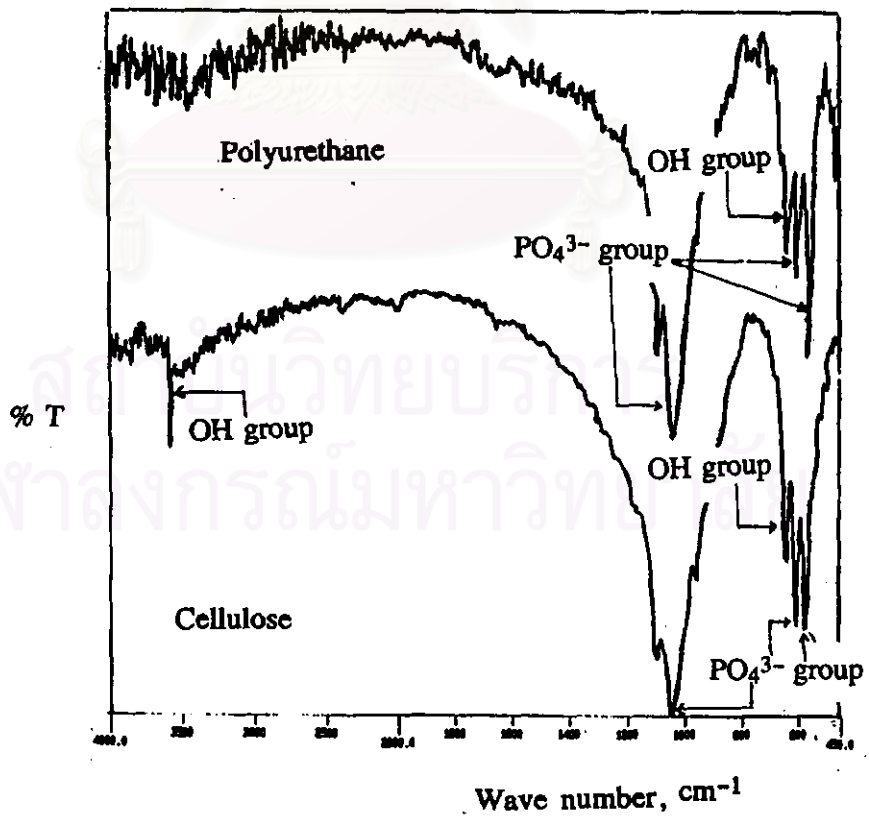


**Fig. 4.29.** Functional groups of TP specimens on different supporter.

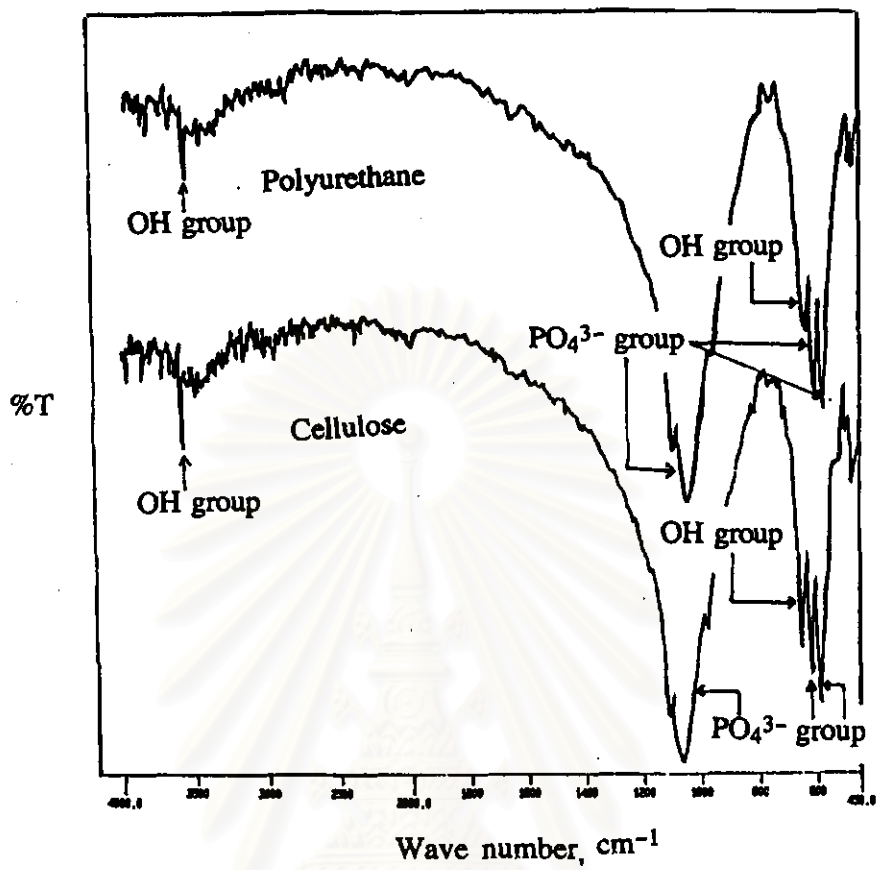


**Fig. 4.30.** Functional groups of CHA specimens on different supporter.

### 4.4.3 Bulk density and porosity of MP, TP and CHA specimens

Bulk density and porosity of all specimens were shown in Table 4.6

**Table 4.6** Apparent porosity and bulk density of specimens.

| Specimens | Apparent porosity %P | Bulk density B, g/cm$^3$ |
|---|---|---|
| MP 60% (Polyurethane) | 56.61 | 1.36 |
| MP 70% (Cellulose) | 54.54 | 1.41 |
| MP 70% (Polyurethane) | 36.15 | 1.98 |
| TP 47.5% (Cellulose) | 61.43 | 1.21 |
| TP 47.5% (Polyurethane) | 55.26 | 1.41 |
| CHA 47.5% (Cellulose) | 66.45 | 1.05 |
| CHA 47.5% (Polyurethane) | 56.83 | 1.35 |

From these results, specimens replicated from cellulose had tendency to have more porosity than those from polyurethane. MP specimens compared with TP and CHA specimens were found that MP had lower porosity. Because of the lower viscosity of slips. These made the slip easily infiltrating into cellulose sponges or polyurethane foams. So, TP and CHA had more porosity. From

above Table, CHA specimens had porosity not different from TP. From the experiment, we may deduced that porosity is inverse proprotion with slip viscosity. The porosity of specimens increase when slip viscosity decrease. Bulk density of specimens increase when porosity decreases.

### 4.4.4 Pore size

#### 4.4.4.1 Mercury Porosimetry

Determining pore volume distribution by mercucy intrusion, the non wetting liquid (mercury in this test method) must be forced into the pores by the application of external pressure. The size of the pore that are intruded is inversely proportional to the applied pressure. When a cylindrical pore model is assumed, the relationship between pressure and size is :

$$d = \frac{-4\,\gamma \cos\theta}{P}$$

Where

d = apparent diameter of pore being intruded,
$\gamma$ = surface tension of the mercury,
$\theta$ = contact angle between the mercury and solid,
P = absolute presure causing the instrusion

The volume of the intruded pores is determined by measuring the volume of mercury that is forced into them at various pressures. A single-pore size distribution determination involves increasing the pressure, either continuously or step-wise, and recording the measured intruded volume.

For this method, average pore diameter of these specimens were reported in Table 4.7. Cumulative intrusion vs. diameter plot of these specimens were shown in Fig. 4.31–4.37.

**Table 4.7.** Average pore diameter of MP, TP and CHA porous specimens from mercury porosimeter

| Materials | Contact angle of mercury (deg) | Surface tension (dyn/cm) | Mean pore diameter (Volume) nm. | Mean pore diameter (volume) μm. |
|---|---|---|---|---|
| MP 60% (Polyurethane) | 130 | 485 | 16672 | 1.67 |
| MP 70% (Cellulose) | 130 | 485 | 12209 | 1.22 |
| MP 70% (Polyurethane) | 130 | 485 | 9087 | 0.91 |
| TP 47.5% (Cellulose) | 130 | 485 | 130925 | 13.09 |
| TP 47.4% (Polyurethane) | 130 | 485 | 489084 | 48.91 |
| CHA 47.5% (Cellulose) | 130 | 485 | 4579 | 0.46 |
| CHA 47.5% (Polyurethane) | 130 | 485 | 89017 | 8.90 |

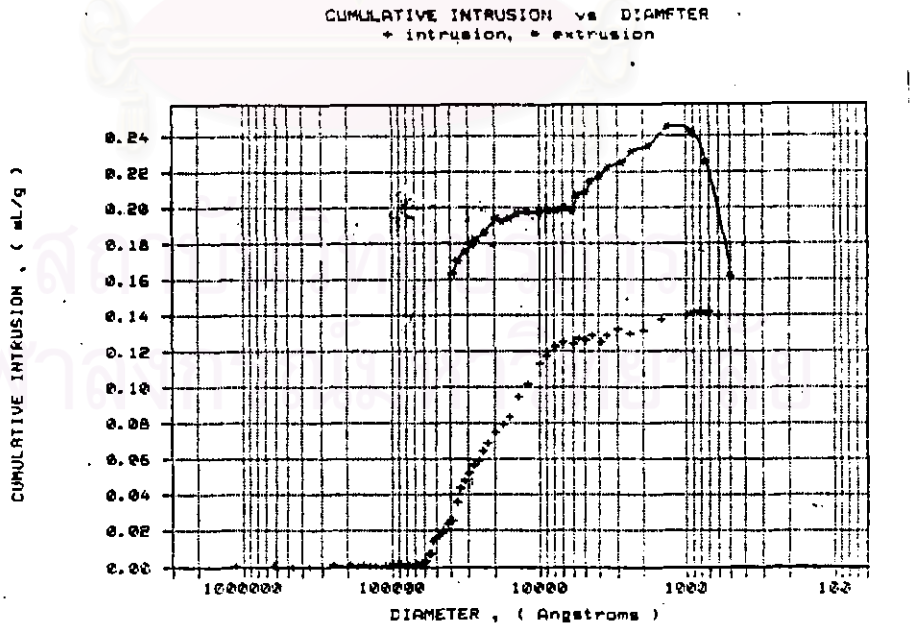


**Fig. 4.31.** Cumulative intrusion vs diameter of MP 60% (Polyurethane)

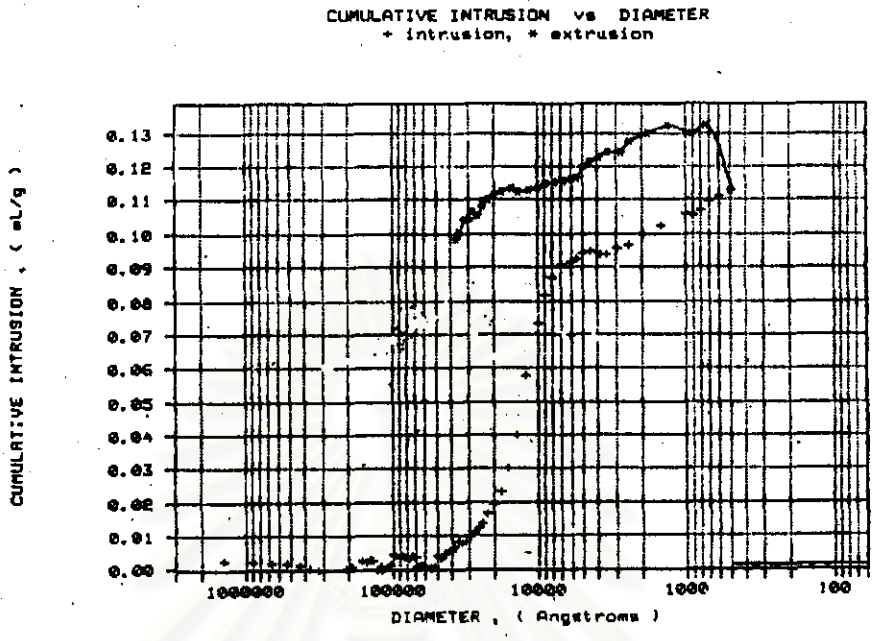


**Fig. 4.32.** Cumulative intrusion vs diameter of MP 70% (Cellulose)

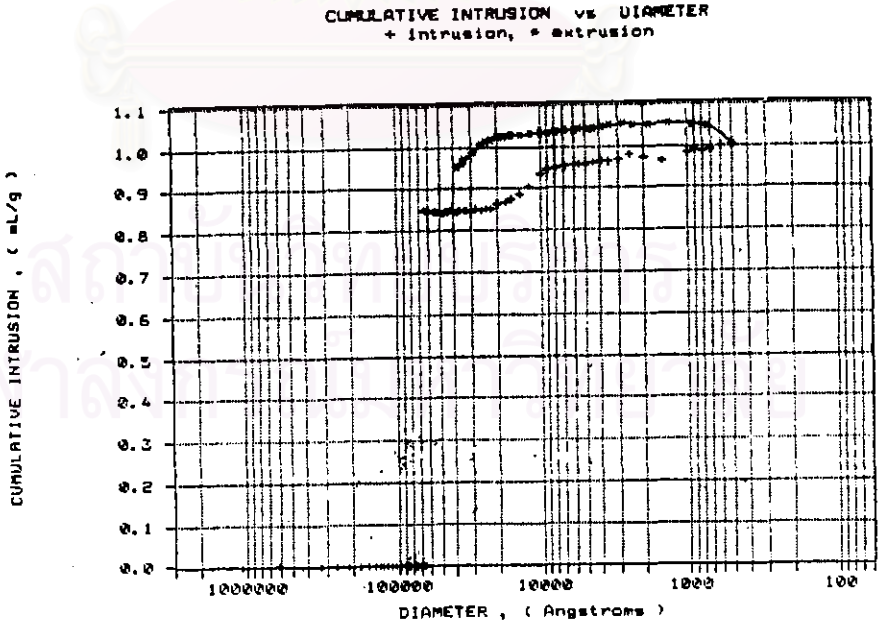


**Fig. 4.33.** Cumulative intrusion vs diameter of MP 70% (Polyurethane)

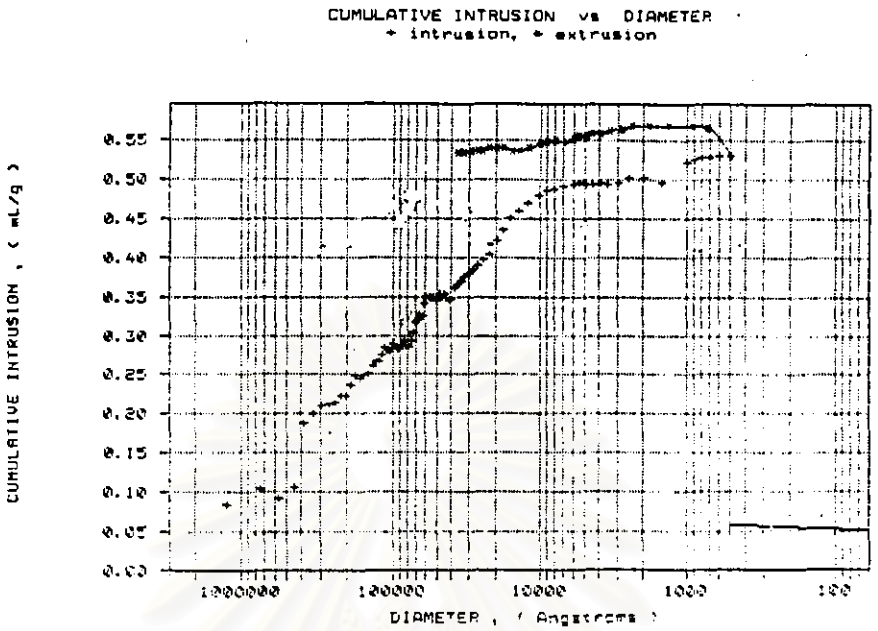


**Fig. 4.34.** Cumulative intrusion vs diameter of TP (Cellulose)

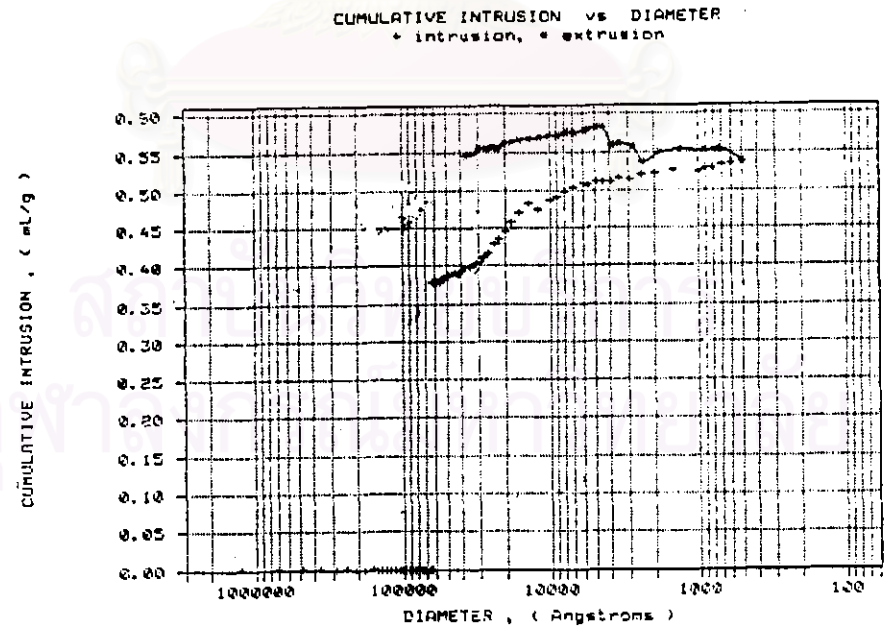


**Fig. 4.35.** Cumulative intrusion vs diameter of TP (Polyurethane)

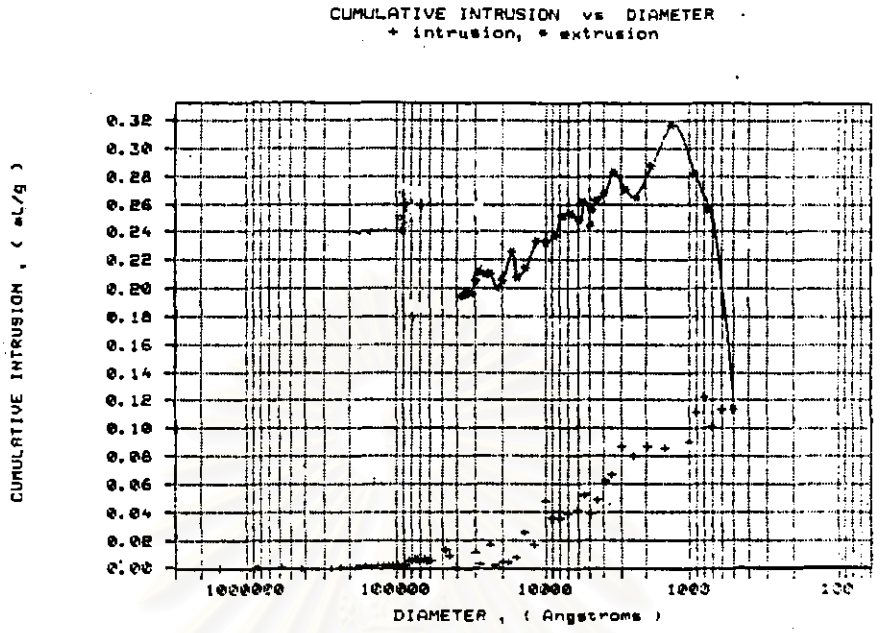


**Fig. 4.36.** Cumulative intrusion vs diameter of CHA (Cellulose)

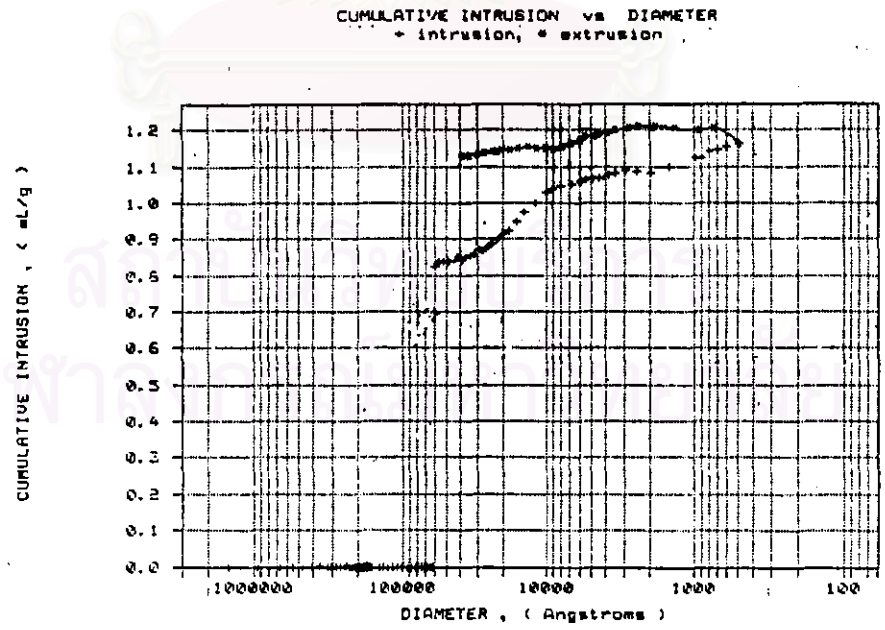


**Fig. 4.37.** Cumulative intrusion vs diameter of CHA (Polyurethane)

Pore size values from mercury porosimeter was very small. Pores of these porous specimens can be seen by nakedeye. So, these pore size must be over 100 μm. This error may come from limiting of instrument. The range of apparent diameters of pores for which it is appliciable is fixed by operant pressure range of the testing instrument. This range is typically between apparent pore entrance diameter of about 360 μm. and 0.063 μm. (3nm.) So, the detected pores may be micropores in specimen. When these data were compared together. It's found that the smaller micropore, the better compressive strength. Micropores size of TP > CHA > MP in the bodies of specimens replicated from polyurethane foam. So compressive strength of MP should more than TP and CHA. But this tendency wasn't in the specimens replicated from cellulose sponge owing to the discreted pores in cellulose structure.

### 4.44.2 Scanning electron microscope (SEM)

Pore size and pore structure of MP, TP, CHA (in cellulose and polyurethane) were investigated and shown in Fig. 4.38–4.44. Pore sizes measured from scanning electron micrograph was shown in Table 4.7 Pores were interconnecting pores. Pore sizes of specimens replicated from cellulose sponge had larger pore sizes than those from polyurethane foam.

**Table 4.8.** Pore size from scanning electron micrograph.

| Materials | Range of pore sizes (μm.) |
|---|---|
| MP 60% (Polyurethane) | 1070–180 |
| MP 70% (Cellulose) | 1130–440 |
| MP 70% (Polyurethane) | 1020–490 |
| TP 47.5% (Cellulose) | 1250–176 |
| TP 47.5% (Polyurethane) | 530–270 |
| CHA 47.5% (Cellulose) | 2050–1346 |
| CHA 47.5% (Polyurethane) | 1050–460 |

Porous hydroxyapatite specimens had pore size ranging from 180 μm. to 2050 μm.

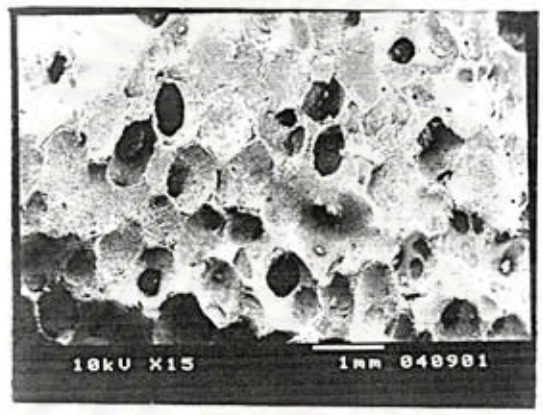




**Fig. 4.38.** Scanning electron micrograph of MP 60% (Polyurethane)

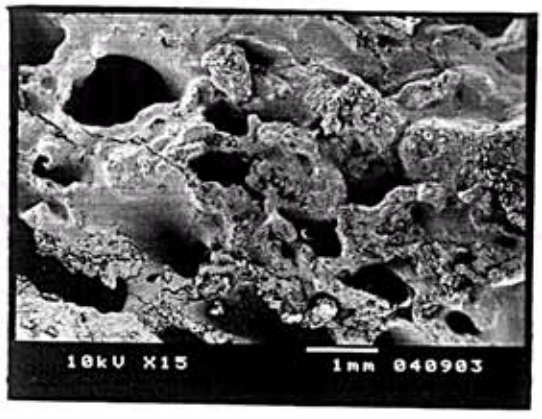


**Fig. 4.39.** Scanning electron micrograph of MP 70% (Cellulose)

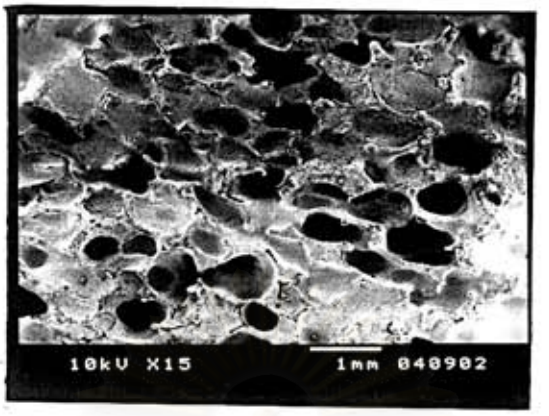


**Fig. 4.40.** Scanning electron micrograph of MP 70% (Polyurethane)

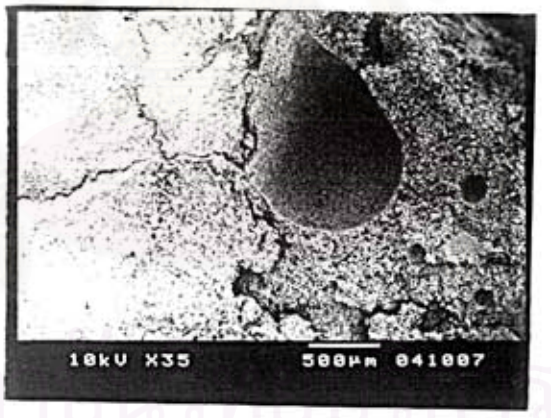


**Fig. 4.41.** Scanning electron micrograph of TP (Cellulose)

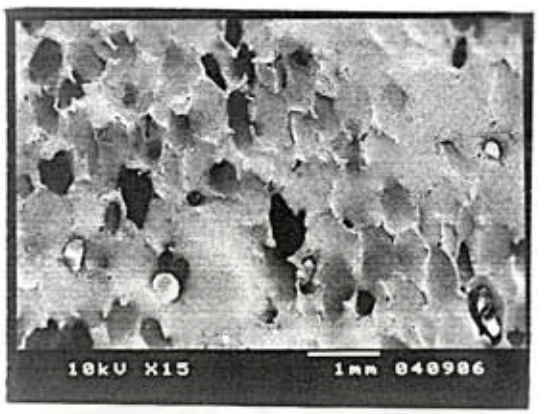


**Fig. 4.42.** Scanning electron micrograph of TP (Polyurethane)

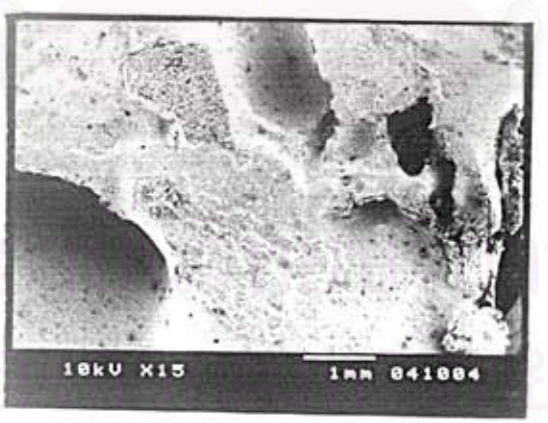


**Fig. 4.43.** Scanning electron micrograph of CHA (Cellulose)

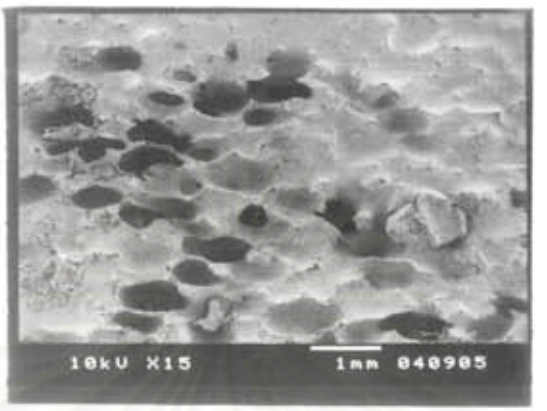


**Fig. 4.44.** Scanning electron micrograph of CHA (Polyurethane)

### 4.4.5. Compressive strength

Compressive strength of specimens were shown in Table 4.9

**Table 4.9.** Compressive strength of specimens

| Specimens | Compressive strength (MPa) |
|---|---|
| MP 60%Polyurethane) | 8.52±0.75 |
| MP 70% (Cellulose) | 14.73±0.15 |
| MP 70% (Polyurethane) | 19.40±0.42 |
| TP 47.5% (Cellulose) | 2.77±0.25 |
| TP 47.5% (Polyurethane) | 6.91±0.18 |
| CHA 47.5% (Cellulose) | 2.92±0.20 |
| CHA47.5%(Polyurethane) | 8.24±0.22 |

Results from Table 4.8 showed that compressive strength of MP> CHA>TP in both replicated specimens. But MP had very high compressive strength than the others because of adding sintering aid $Ca(PO_3)_2$ which improved strength of specimens. Compressive strength of TP was lower than CHA because of lower in solid content of slip system.